Chapter 8
Methods for Creep Rupture Analysis—Previous Attempts and New Challenges

Zbigniew L. Kowalewski

Abstract The chapter presents selected methods of creep analysis with special emphasis on damage development. It is divided into three main sections. In the first one some previous methods of creep rupture analysis are described. The attention is focused on certain kind of uniaxial creep characterisation of materials, namely, an influence of prior deformation on creep behaviour. Subsequently, the results from creep tests under complex stress states are presented together with theoretical approaches commonly used to their description. In the second section a comprehensive historical survey concerning advances in modelling of creep constitutive equations is discussed. The third section illustrates selected new concepts of damage development due to creep on the basis of data captured from the own experimental programme.

Keywords Creep · Creep damage · Prior deformation · Constitutive equations · Complex stress states · Non-destructive testing

8.1 Introduction

Typical creep phenomenon occurs as a result of long term exposure to high levels of stress that are below the yield point of the material. It is more severe in materials that are subjected to elevated temperature for long periods, and near melting point. It always becomes faster with temperature increase. The rate of this deformation is a function of the material properties, exposure time, exposure temperature and the applied structural load. Depending on the magnitude of the applied stress and its duration, the deformation may become so large that a component can no longer

Z.L. Kowalewski (✉)
Institute of Fundamental Technological Research,
Ul. Pawinskiego 5B, 02-106 Warsaw, Poland
e-mail: zkowalew@ippt.pan.pl

H. Altenbach et al. (eds.), *From Creep Damage Mechanics to Homogenization Methods*, Advanced Structured Materials 64,
DOI 10.1007/978-3-319-19440-0_8

perform its function. Creep is usually of concern to engineers and metallurgists when evaluating components that operate under high stresses or high temperatures. The temperature range in which creep deformation may occur differs in various materials. For example, tungsten requires a temperature in the thousands of degrees before creep deformation can occur while lead will creep near the room temperature 20 °C. The effects of creep deformation generally become noticeable at approximately 30 % of the melting point (as measured on a thermodynamic temperature scale such as Kelvin) for metals and 40 % of melting point for alloys. For typical creep curve one can distinguish three stages. In the initial stage, or primary creep, the strain rate is relatively high, but slows with increasing time. This is due to work hardening. The strain rate eventually reaches a minimum and becomes near constant. This is due to the balance between work hardening and thermal softening. This stage is known as secondary or steady-state creep. In tertiary creep, the strain rate exponentially increases with stress because of necking phenomena.

Creep leads to the development of material damage process. There are two essential periods of such process:

- damage developing without microscopically visible cracks due to the nucleation process and growth of the microvoids, and
- propagation of the dominant fissure up to failure.

At the end of the first stage, the macroscopically observed crack takes place in form of one or several fissures. In the second stage of the rupture process the dominant fissure propagates decreasing, as a consequence, loading admissible capacity of a construction element and leading finally to its failure. In most cases the duration of the second stage of damage process is negligible short in comparison to the exploitation time of an element. Experiments concerning the processes of microcrack nucleation and growth, which are responsible for the failure of materials during creep, exhibit that failure mechanisms can be divided into the three following types (Hayhurst 1972, 1983; Dyson and Gibbons 1987; Abo El Ata and Finnie 1972; Browne et al. 1981; Ashby et al. 1979): brittle, ductile and mechanism being their combination. For brittle failure mechanism the microdefects are created and developed on the grain boundaries perpendicular to the maximum principal tension stress. During ductile failure mechanism the microdefects are created on the grain boundaries and they are developing due to grain boundary slides. Brittle failure mechanism is usually dominant in the case of polycrystalline materials tested at low levels of the uniaxial stress states. Material degradation during this mechanism has the intergranular character. At high stress levels the rupture takes place mainly due to the ductile failure mechanism, for which the damages have a transgranular character and develop due to the slides passing through the grains. It is well known that there are no exact values, which can be treated as the limits for particular failure mechanism domination. For majority of real exploitation loading conditions the failure mechanism seems to be a combination of the simultaneously developing brittle and ductile failure mechanisms.

8.1.1 Uniaxial Creep Tests—Tool for Initial Material Characterization

During manufacturing and exploitation processes most engineering structures or some their elements are subjected to deformation. Therefore, it is important from engineering point of view to know the influence of this deformation on such different material properties at high temperatures as minimum creep rate, ductility, lifetime, rupture and crack propagation. It has been found that plastic deformation at both room and elevated temperatures prior to creep testing has either beneficial or detrimental effect on the material properties (Dyson and Rodgers 1974; Dyson et al. 1976; Kowalewski 1991a, 1992; Marlin et al. 1980; Murakami et al. 1990; Ohashi et al. 1986; Pandey et al. 1984; Rees 1981; Trąmpczyński 1982; Wilson 1973; Xia and Ellyin 1993). Although the problem has been previously studied experimentally for several materials, only limited amount of available data reflects the influence of plastic predeformation on creep process up to rupture (Dyson and Rodgers 1974; Dyson et al. 1976; Marlin et al. 1980; Pandey et al. 1984; Trąmpczyński 1982). It is well known that the problem is particularly important during fabrication or assembly processes, where a number of materials used in critical elements of engineering structures may receive such cold work, and as a consequence, it may change significantly their lifetime. Up to now the amount of experimental data is still insufficient to estimate exactly whether the increase or decrease of creep strengthening occurs up to a certain amount of prior deformation only, or whether this creep property is in some way proportional to the amount of predeformation. Thus, in order to achieve better understanding of this problem further systematic investigations are required.

In this paper in order to identify an influence of prior plastic deformation on the basic creep parameters the results of uniaxial tensile tests obtained for aluminium alloy will be presented.

8.1.2 Multiaxial Creep Tests—Advanced Characterization of Materials

The results from uniaxial creep tests are not able to reflect complex material behaviour. Therefore, many efforts are focused on tests carrying out under multiaxial loading conditions. Such experiments are very difficult not only in execution but also in elaboration of the results.

A description of creep process requires the essential interrelations among stress, strain, and time. The well known method depicting these interrelation-ships under complex stress states, first proposed by McVetty (1934), is through isochronous stress-strain curves obtainable from the standard creep curves. Since that time, many graphical methods of the creep data presentation have been elaborated. It has been found that multi-axial creep rupture results are conveniently plotted in terms of isochronous surfaces (Piechnik and Chrzanowski 1970; Leckie and Hayhurst 1977; Chrzanowski and Madej 1980; Hayhurst et al. 1980; Litewka and

Hult 1989; Kowalewski et al. 1994; Kowalewski 2004) being loci of constant rupture time in a stress space. Such approach especially simplifies theoretical and experimental creep results analysis giving comprehensive graphical representation of material lifetime, and therefore, it will be used as a tool for the creep data presentation. The paper demonstrates comparison of experimental creep data achieved for pure copper (Kowalewski 1995, 1996; Lin et al. 2005) with the results for 2017 aluminium alloy obtained. Theoretical approach for determination of the isochronous surfaces will be discussed, and the data from creep tests will be used to illustrate how to construct an experimental form of such surfaces.

8.1.3 New Concepts of Creep Analysis

Nowadays many new approaches and testing techniques are used for damage assessments. Among them one can generally distinguish destructive (Hayhurst 1972, 1983; Krauss 1996; Lin 2003; Trąmpczyński and Kowalewski 1986; Dietrich and Kowalewski 1997; Kowalewski 2002), and non-destructive methods (Sablik and Augustyniak 1999; Narayan GR 1975; Fel et al. 2001; Martínez-Ona and Pérez 2000; Ogi et al. 2000). Having the parameters of destructive and non-destructive methods for damage development evaluation it is instructive to analyze their variation in order to find possible correlations. This is because of the fact that typical destructive investigations, like creep or standard tension tests, give the macroscopic parameters characterizing the lifetime, strain rate, yield point, ultimate tensile stress, ductility, etc. without sufficient knowledge concerning microstructural damage development and material microstructure variation. On the other hand, non-destructive methods provide information about damage at a particular time of the entire working period of an element, however, without sufficient information about the microstructure and how it varies with time. Therefore, it seems reasonable to plan future damage development investigations in the form of interdisciplinary tests connecting results achieved using destructive and non-destructive methods with microscopic observations in order to find mutual correlations between their parameters. This issue will be demonstrated on the basis of last own results.

8.2 Previous Attempts of Creep Analysis—Selected Examples of Uniaxial and Biaxial Tests

8.2.1 Analysis of Prior Deformation Effect on Creep Under Uniaxial Loading Conditions

It is commonly known that standard tensile creep tests are most often used to characterize a majority of engineering materials. In this section such kind of material

testing was applied to identify an influence of prior cold work on creep of 2017 aluminium alloy. Thin-walled tubular specimens of 40 [mm] gauge length, 22 [mm] internal diameter, 0.75 [mm] wall thickness and 140 [mm] total length were used in all tests. The experimental programme comprised creep tests under uniaxial tension carried out at two different temperatures 423 and 473 K. Creep tests were performed for the material in the as-received state and for the same material plastically prestrained at the room temperature. The aluminium alloy specimens were prestrained up to 1.0, 2.0, 6.0 and 8.0 % for both creep test temperatures taken into account.

Investigations of the effect of prior plastic deformation on subsequent creep process were carried out according to the following procedure. First of all, each thin-walled tubular specimen was proportionally deformed up to the selected value of plastic prestrain by uniaxial tension at the room temperature using an Instron testing machine, and then unloaded. Subsequently, each specimen was mounted at the standard creep testing machine, heated uniformly at the chosen test temperature for 24 [h] prior to creep testing, and then subjected to the constant stress level depending on the creep testing temperature. Both creep stress levels selected for tested material were smaller than the value of yield point of the material at the considered temperatures. Diagram of the experimental procedure is schematically presented in Fig. 8.1.

The experimental results for aluminium alloy are presented in Fig. 8.2. As it is clearly seen from this figure, creep process under constant stress is generally affected by prior plastic strain at the room temperature. Cold work preceding the creep induced hardening effect expressed by significant decrease of the minimum creep rate, Fig. 8.3. Similar effect was earlier observed by Trąmpczyński (1982) and Kowalewski (1991a) who tested copper. Taking into account the recovery creep theory based on the Orowan's equation in the following form

$$\mathrm{d}\sigma = \left(\frac{\partial \sigma}{\partial \varepsilon}\right)\mathrm{d}\varepsilon + \left(\frac{\partial \sigma}{\partial t}\right)\mathrm{d}t \tag{8.1}$$

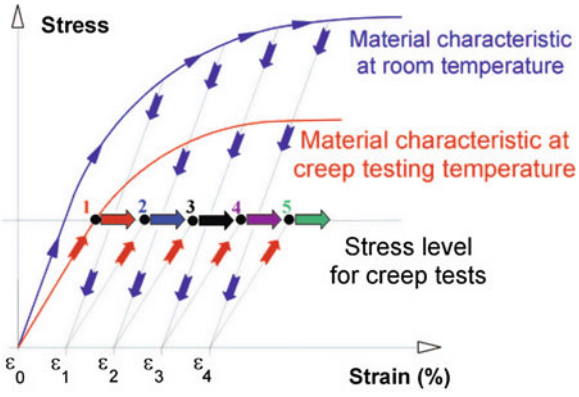

Fig. 8.1 Scheme of the experimental programme (2017 aluminium alloy tested under 300 MPa at 423 K, and under 200 MPa at 473 K—$\varepsilon_0 = 0\,\%$, $\varepsilon_1 = 1.0\,\%$, $\varepsilon_2 = 2.0\,\%$, $\varepsilon_3 = 6.0\,\%$, $\varepsilon_4 = 8.0\,\%$)

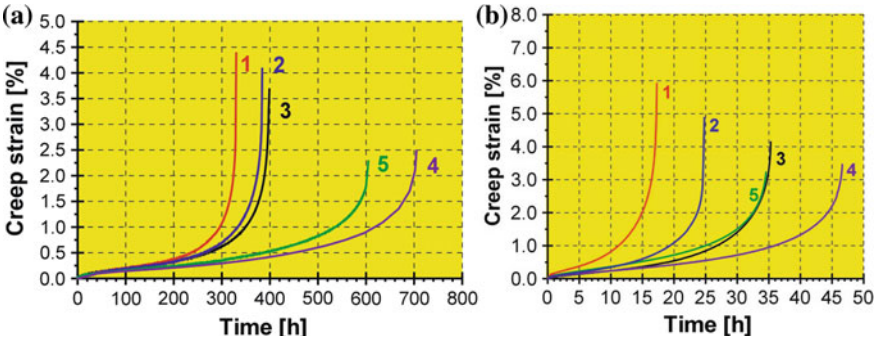

Fig. 8.2 Creep curves of 2017 aluminium alloy at: **a** σ = 300 MPa, T = 423 K; **b** σ = 200 MPa, T = 473 K (*1* material in the as-received state; *2–5* material prestrained up to 1.0, 2.0, 6.0, 8.0 %, respectively (Kowalewski 2005)

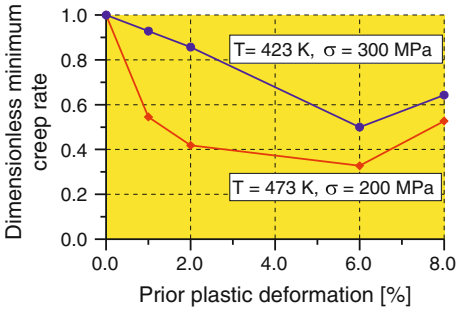

Fig. 8.3 Variation of the dimensionless minimum creep rate due to prior plastic deformation for aluminium alloy (Minimum creep rates of nonprestrained material are used as the reference values (Kowalewski 2005))

this is an expectable effect. According to this theory a balance between the recovery rate $\partial\sigma/\partial t$ and the rate of strain hardening $\partial\sigma/\partial\varepsilon$ is responsible for constant value of strain rate observed in the second period of the creep process.

Plastic predeformation of a material generates dislocations, the density of which depends on the prestrain amount. Therefore, the plastically prestrained material should creep at lower rate during second period of the process than the nonprestrained one. Taking into account the results of tests carried out at 423 K, Fig. 8.3, it is easy to note that the strain hardening effect observed exhibits gradual increase with the plastic predeformation increase only up to the prior plastic deformation close to 6 %. Over this value the hardening effect expressed by decrease of the secondary creep rate was also remarkable, but its amount was not proportional to the magnitude of prestraining. In the tests carried out for copper at 473 K similar tendency can be observed.

On the basis of the results achieved for 2017 aluminium alloy it may be concluded that the tensile plastic prestrains decrease the secondary creep rate, but the magnitude of this decrease is not proportional to the amount of tensile plastic prestrain. Such behaviour cannot be predicted by the recovery creep theory.

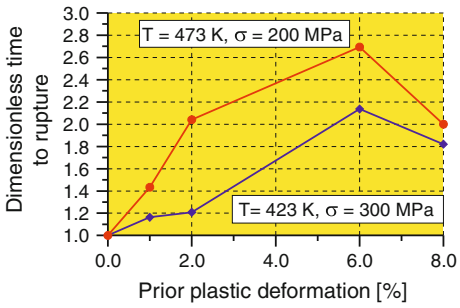

Fig. 8.4 Variation of the dimensionless time to rupture due to prior plastic deformation for aluminium alloy (Times to creep rupture of nonprestrained material are used as the reference values (Kowalewski 2005))

Lifetime extension was obtained for prestrained aluminium alloy at both temperatures considered, Fig. 8.4. For relatively small values of prior plastic deformation (up to 6 %) the mutual relation between the lifetime and the amount of prior plastic deformation was almost proportional. For higher values of plastic prestraining the lifetime extension can be also observed in comparison to the lifetime achieved for the nonprestrained material, however, in these cases mutual relation between the lifetime and the amount of prior plastic deformation was not proportional. It means that for higher magnitudes of plastic deformation (>6 %) the creep lifetime becomes to be smaller, and for sufficiently high magnitude it can reach the lower value than that obtained for the material tested in the as-received state.

Prior plastic deformation also can change the duration of typical creep stages (Table 8.1). The duration of the primary creep period was reduced, in practice, independently on the amount of prior plastic deformation. The duration of secondary creep stage was increased with the increase of the plastic prestrain magnitude.

The ductility during creep was also strongly affected by the prior plastic deformation at room temperature. For both temperatures considered an essential reduction of the total creep strain at rupture was observed.

8.2.2 Creep Tests Under Complex Stress States

The vast majority of the creep-to-rupture investigations have been carried out under uniaxial stress states (Norton 1929; Malinin and Rżysko 1981; Rabotnov 1969; Gittus 1975). Results of such tests have been subsequently used to deter-

Table 8.1 Creep parameters determined from tensile creep tests of 2017 aluminium alloy

	σ = 300 (MPa), T = 432 (K)					σ = 200 (MPa), T = 432 (K)				
ε (%)	0	1.0	2.0	6.0	8.0	0	1.0	2.0	6.0	8.0
$\dot{\varepsilon} \times 10^{-5}$ (1/h)	1.4	1.3	1.2	0.7	09	5.5	3.0	2.3	1.8	2.9
t_I (h)	70	60	50	50	40	1	2	2	4	3
t_{II} (h)	160	180	200	260	250	6	9	12.5	17	12
t_R (h)	330	384	399	705	601	17.3	24.8	35.3	46.6	34.6

mine material constants existing in different theoretical models with the objective to precisely reflect creep behaviour of the material considered. These models are often generalized into multi-axial stress states under assumption of the isotropy of a body examined (Hayhurst 1983; Garofalo 1965; Kachanov 1958; Odqvist 1966). However, the isotropic materials exist in practice rather seldom since manufacturing processes used to produce semi-manufactures, such as rods, tubes, sheets etc., induce anisotropy which cannot be often remove by any heat treatment subsequently applied. In some cases the material can be isotropic in sense of plastic parameters such as yield limit and ultimate tensile strength, but during creep can exhibit anisotropic properties (Kowalewski 1991a, b). In these situations carrying out only uni-axial creep tests to obtain material constants for constitutive model describing material behaviour may lead to significant errors.

In this section the results of biaxial creep tests will be presented to identify phenomena that should be reflected during elaboration of reasonable constitutive equations.

The materials investigated were electrolytic copper of 99.9 % purity and 2017 aluminium alloy (notation according to ASTM). Creep investigations were carried out on thin-walled tubular specimens (40 mm gauge length, 140 mm total length, 22 mm internal diameter, 1.5 mm (copper specimens) or 0.75 mm (aluminium alloy specimens) wall thickness in the gauge length region) with the use of the biaxial creep testing machine enabling realisation of plane stress conditions by simultaneous loading of the specimens by an axial force and twisting moment at elevated temperature.

The experimental programme comprised creep tests up to rupture for copper and aluminium alloy specimens subjected to biaxial stress state obtained by various combinations of tensile and torsional stresses: ($\sigma_{12}/\sigma_{11} = 0, \sigma_{12}/\sigma_{11} = \sqrt{3}/3, \sigma_{12}/\sigma_{11} = \infty$. For each material tests were carried out at three effective stress levels (σ_e): 70.0; 72.5; and 75.0 [MPa] in the case of copper, and 280.0; 300.0; and 320.0 [MPa] in the case of aluminium alloy. The effective stress was defined in the following form:

$$\sigma_e = \left(\frac{3}{2} S_{ij} S_{ij}\right)^{\frac{1}{2}} = \left(\sigma_{11}^2 + 3\sigma_{12}^2\right)^{\frac{1}{2}}, \tag{8.2}$$

where S_{ij}—stress deviator, σ_{11}—axial stress, σ_{12}—shear stress.

Before creep test each specimen was heated uniformly at the test temperature (523 K in the case of copper, and 423 K in the case of aluminium alloy) for 24 h. Creep investigations were carried out until rupture of the specimens was achieved giving as a consequence whole creep curves.

8.2.2.1 Creep Results of Pure Copper

The creep curves up to rupture for copper are presented in Fig. 8.5. The effective creep strain was defined by the relation in the following form:

$$\varepsilon_{\mathrm{e}} = \left(\frac{2}{3}\varepsilon_{ij}\varepsilon_{ij}\right)^{\frac{1}{2}} = \sqrt{\varepsilon_{11}^2 + \frac{4}{3}\varepsilon_{12}^2}, \tag{8.3}$$

where ε_{11} and ε_{12} denote axial and shear strain, respectively.

The creep characteristics obtained at the same effective stress but under different stress states exhibit drastic differences for all stress levels considered. In all cases the shortest lifetimes, and moreover, the lowest ductility have been achieved for

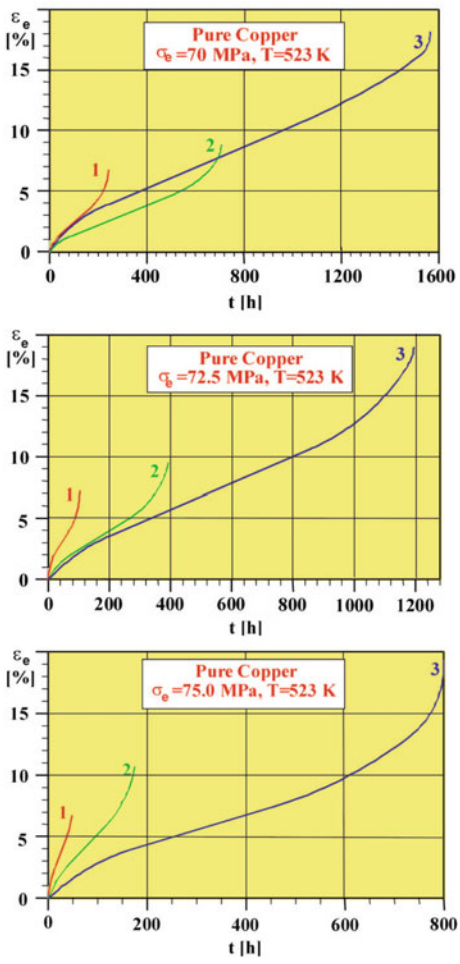

Fig. 8.5 Creep curves for copper: *1* $(\sigma_{12}/\sigma_{11}) = 0$, *2* $(\sigma_{12}/\sigma_{11}) = \sqrt{3}/3$, 3 $(\sigma_{12}/\sigma_{11}) = \infty$

tensioned specimens. The opposite effect was observed for specimens subjected to pure torsion. It has to be emphasized that differences in creep curves due to different loading types applied are great, and they are reflected by variations of the basic creep parameters. Microscopic examination showed that the majority of microcracks were observed at those grain boundaries which were perpendicular to the maximum principal stress. It was confirmed by the shapes of the specimen cross-section in places where rupture occurred. The failure line in each creep rupture test was perpendicular to the maximum principal stress. Since the maximum principal stress was not the same for the same effective stress creep tests, it can be concluded that the resulting variations in lifetimes for the same effective stress tests follow from the differences in magnitude of the maximum principal stress. The longest lifetimes were achieved for pure torsion creep tests for which the maximum principal stresses had the lowest values.

8.2.2.2 Creep Results of 2017 Aluminium Alloy

The creep curves up to rupture for aluminium alloy are presented in Fig. 8.6. Similarly as for copper the creep characteristics of aluminium alloy, obtained at the same effective stress but under different stress states, exhibit drastic differences. In this case, however, the shortest lifetimes, and moreover, the lowest ductility were achieved for specimens subjected to pure torsion. All of the creep parameters which characterise macroscopically creep behaviour prove that the process is a stress state sensitive. More importantly, it has to be noticed that creep behaviour depends on the material type. Analysis of the results for both materials allows to conclude that for some materials tested at the same effective stress the longest lifetime can be achieved under uniaxial tension (e.g. aluminium alloy) whereas for the others under torsion (e.g. copper). Microstructural observations of damage in aluminium alloy showed narrow grain boundary cracks along some grain boundary facets perpendicular to the direction of the maximum principal tension stress in both uniaxial and biaxial stress creep tests. Similar observations were made by Johnson et al. (1962) and later by Hayhurst (1972). These observations suggest that the growth of damage is dependent on the maximum principal tension stress. However, the biaxial tests carried out by both Hayhurst (1972); Johnson et al. (1962) unambiguously showed that the aluminium alloy studied did obey an effective stress criterion. Also, certain aspects of the presented results for aluminium alloy support the latter thesis.

The failure lines of the ruptured specimens were not perpendicular to the maximum principal stress. More importantly, the shortest lifetimes were achieved for the specimens subjected to pure torsion for which, taking into account the same effective stress level, the maximum principal stresses were significantly lower than those at uniaxial tension creep tests applied. The dichotomy between the observation of maximum principal stress controlled damage growth and the observed effective stress rupture criterion is still being discussed, although a suggestion has been made that it is a consequence of tertiary creep being controlled by more than a single damage state variable only (Dyson and Gibbons 1987).

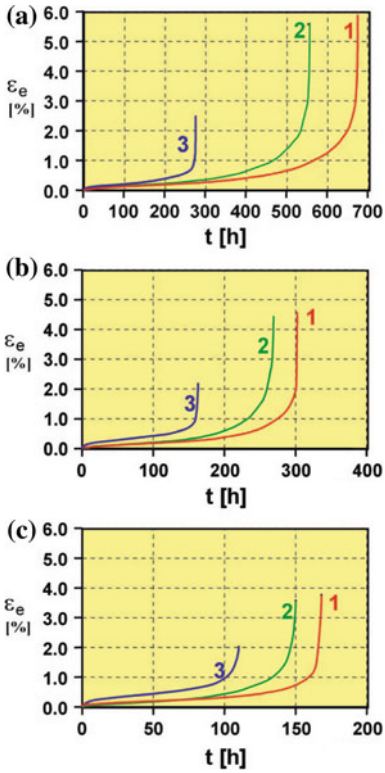

Fig. 8.6 Creep curves for aluminium alloy at 423 K under stress equal to: **a** 280.0 MPa; **b** 300 MPa; **c** 320 MPa; *1* $(\sigma_{12}/\sigma_{11}) = 0$; *2* $(\sigma_{12}/\sigma_{11}) = \sqrt{3}/3$; *3* $(\sigma_{12}/\sigma_{11}) = \infty$

8.2.2.3 Creep Rupture Data Analysis Using Isochronous Surface Concept

The comprehensive presentation and comparison of the experimental data from tests performed at complex stress states procure many difficulties, particularly for stress states being a combination of tension and torsion. In these cases, the data comparison is usually carried out for the effective strains defined in the form of a function of the second invariant of strain tensor, since effects of the first as well as the third invariants are relatively small and they can be often neglected.

Although creep curves in diagrams representing effective strains versus time can be compared, it is difficult to evaluate precisely all differences in material response due to the action of different stress state types. To overcome this deficiency, creep rupture results are commonly presented in the form of isochronous surfaces (Hayhurst 1972, 1983; McVetty 1934; Piechnik and Chrzanowski 1970; Leckie and Hayhurst 1977; Chrzanowski and Madej 1980; Hayhurst et al. 1980; Litewka and Hult 1989; Kowalewski et al. 1994; Kowalewski 1996, 2004; Lin et al. 2005), being loci of constant rupture time in a stress space. This approach especially simplifies theoretical creep results analysis giving the comprehensive graphical representation of the

material lifetime. However, the accurate experimental determination of the shape of these surfaces requires a large number of creep rupture data from tests carried out under complex loading over a wide range of stress levels.

The curves of the same time to rupture determined on the basis of experimental programme are compared with theoretical predictions of the three well known creep rupture hypotheses: (a) the maximum principal stress rupture criterion (8.4), (b) the Huber-Mises effective stress rupture criterion (8.5), (c) the Sdobyrev creep rupture criterion (8.6). For the biaxial stress state conditions, realised in the experimental programme, the rupture criteria mentioned above are defined by the following relations:

$$\sigma_R = \sigma_{max} = \frac{1}{2}(\sigma_{11} + \sqrt{\sigma_{11}^2 + 4\sigma_{12}^2}), \tag{8.4}$$

$$\sigma_R = \sigma_e = \sqrt{\sigma_{11}^2 + 3\sigma_{12}^2}, \tag{8.5}$$

$$\sigma_R = \beta\sigma_{max} + (1 - \beta)\sigma_e \tag{8.6}$$

In Fig. 8.7 the results for copper are shown, while in Fig. 8.8 for aluminium alloy. The curves presented in the normalised co-ordinate system are referred to the rupture time equal to 500 [h]. Tensile stress corresponding to the lifetime of 500 [h] has been selected as the normalisation factor ($\sigma_{R\ 500}$). In the case of copper it was equal to 67.9 [MPa], whereas for aluminium alloy—288 [MPa]. As it is clearly seen for copper, the best description of the experimental data has been achieved for the Sdobyrev creep rupture criterion taken with the coefficient $\beta = 0.4$, calculated on the basis of creep data from tests carried out. The value of β indicates that the damage mechanism governed by the effective stress as well as the maximum principal stress played a considerable role in the creep rupture of the copper tested. Contrary to the results achieved for copper, the best fit of the aluminium alloy data is obtained using the effective stress rupture criterion. It has to be noting however, that the lifetimes predicted by this criterion are still quite far from experimental data.

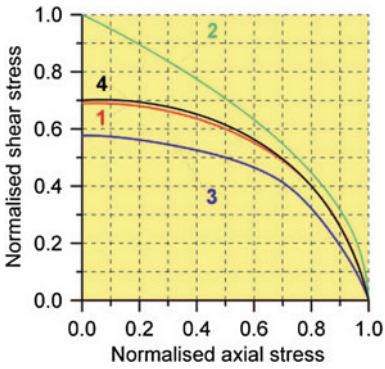

Fig. 8.7 Comparison of the isochronous creep rupture surfaces ($t_R = 500$ [h]) determined for copper (*1* experimental results; *2–4* theoretical predictions using the maximum principal stress criterion; the effective stress criterion; and the Sdobyrev criterion, respectively)

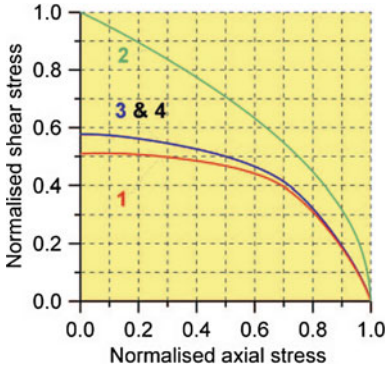

Fig. 8.8 Comparison of the isochronous creep rupture surfaces ($t_R = 500$ [h]) determined for aluminium alloy (*1* experimental results; *2–4* theoretical predictions using the maximum principal stress criterion; the effective stress criterion; and the Sdobyrev criterion, respectively)

8.3 A Short Survey on Advances in Modelling of Creep Damage Development

A definition of damage measure is treated as the essential problem taking place in creep rupture analysis. In 1958 Kachanov has introduced a scalar measure of damage in the form of parameter of cross-section continuity, which becomes to be 1 at the beginning of the deformation process and 0 at a localized failure of the material (Kachanov 1958). It corresponds to the assumption that the load is only carrying by the effective part of the specimen cross-section being a difference between the initial cross-section and the damage area, i.e. the area resulted from the sum of all voids or fissures areas. Rabotnov (1969) modified the Kachanov's damage measure giving more convenient measure being the complementary parameter to that proposed by Kachanov. It is defined in the following form

$$\omega = 1 - \psi = \frac{A_0 - A}{A_0}, \qquad 0 \le \omega \le 1 \tag{8.7}$$

and physically can be interpreted as the area of all defects referred to the undamaged initial cross-sectional area. Using this damage parameter the creep constitutive equation set for uniaxial stress state can be written in the following normalised form:

$$\frac{\dot{\varepsilon}}{\dot{\varepsilon}_0} = \frac{1}{(1-\omega)^m}\left(\frac{\sigma}{\sigma_0}\right)^n, \qquad \frac{\dot{\omega}}{\dot{\omega}_0} = \frac{1}{(1-\omega)^\eta}\left(\frac{\sigma}{\sigma_0}\right)^\nu, \tag{8.8}$$

where $n, m, \nu, \eta, \dot{\varepsilon}_0, \dot{\omega}_0, \sigma_0$ are material constants.

For constant stress level it is easy to integrate the equations in set (8.8) to give the time variations of strain and damage. By applying the rupture condition $\omega = 1$, it is possible to determine time to rupture t_R (Leckie and Hayhurst 1977).

The generalisation of Eq. (8.8) to multiaxial stresses, proposed by Leckie and Hayhurst (1977), has been achieved by making the assumption that the influence of continuum damage on the deformation rate process is of a scalar character, and by the introduction of the homogeneous stress function which reflects the stress state effects on the time to rupture. Equation (8.8) can then be written as:

$$\frac{\dot{\varepsilon}_{ij}}{\dot{\varepsilon}_0} = \frac{3}{2}\left(\frac{\sigma_{\mathbf{e}}}{\sigma_0}\right)^{n-1}\left(\frac{S_{ij}}{\sigma_0}\right)\frac{1}{(1-\omega)^n}, \tag{8.9}$$

$$\frac{\dot{\omega}}{\dot{\omega}_0} = \Delta^{\nu}\frac{1}{(1+\eta)(1-\omega)^{\eta}}, \tag{8.10}$$

where $\Delta = \Delta(\sigma_{ij}/\sigma_0) = \sigma_{\max}/\sigma_0$ for copper, and $\Delta = \Delta(\sigma_{ij}/\sigma_0) = \sigma_{\mathrm{e}}/\sigma_0$ for aluminium alloys. Integration of the damage evolution equation (8.10) for the following boundary conditions: $\omega = 0, t = 0$ and $\omega = 1, t = t_{\mathbf{R}}$, yields after normalisation to the relation describing time to rupture in the form:

$$\frac{t_{\mathrm{R}}}{t_0} = \frac{1}{\Delta^{\nu}} \tag{8.11}$$

Substitution of $t_{\mathrm{R}} = t_0$ in Eq. (8.11) gives the equation of the isochronous surface.

It has been found convenient to present the rupture results in terms of the isochronous surface representing stress states with the same rupture times. According to (Johnson et al. 1956, 1962), the rupture criteria for aluminium alloy and pure copper appear to represent the extremes of material behaviour, since the isochronous surface for many metals lies somewhere between these criteria. They have shown that the dependence of the rupture time upon the nature of the applied stress system for an aluminium alloy can be described by the octahedral shear stress criterion, whereas for pure copper—by the maximum principal stress criterion. In spite of the fact that these observations have been made on the basis of a relatively limited amount of the experimental data, and in certain cases did not give precise description of rupture, they are still influencing the process of developing new creep damage models (Hayhurst et al. 1980; Litewka and Hult 1989; Kowalewski et al. 1994; Kowalewski 2004; Lin et al. 2005; Dyson and McLean 1977; Sdobyrev 1959).

Multiaxial creep constitutive equations (8.9) and (8.10) describe phenomenological aspect of the process. The material constants in this set do not have clear physical meaning. Therefore, the physically-based constitutive equations have been developed in the last decades. Typical example of such equation set has been proposed by Kowalewski et al. (1994) in the following form:

$$\begin{aligned}
\frac{\mathrm{d}\varepsilon_{ij}}{\mathrm{d}t} &= \frac{3}{2}\frac{A}{(1-\omega_2)^n}\frac{\bar{S}_{ij}}{\sigma_\mathrm{e}}\sinh\left(\frac{B\sigma_\mathrm{e}(1-H)}{1-\Phi}\right),\\
\frac{\mathrm{d}H}{\mathrm{d}t} &= \frac{h}{\sigma_\mathrm{e}}\frac{A}{1-\omega_2}\sinh\left(\frac{B\sigma_\mathrm{e}(1-H)}{1-\Phi}\right)\left(1-\frac{H}{H^*}\right),\\
\frac{\mathrm{d}\Phi}{\mathrm{d}t} &= \frac{K_\mathrm{c}}{3}(1-\Phi)^4,\\
\frac{\mathrm{d}\omega_2}{\mathrm{d}t} &= \frac{DA}{(1-\omega_2)^n}\left(\frac{\sigma_1}{\sigma_\mathrm{e}}\right)^n N\sinh\left(\frac{B\sigma_\mathrm{e}(1-H)}{1-\Phi}\right),
\end{aligned} \tag{8.12}$$

where A, B, H^*, h, K_c, D—material constants and n is given by

$$n = \frac{B\sigma_\mathrm{e}(1-H)}{1-\Phi}\coth\left(\frac{B\sigma_\mathrm{e}(1-H)}{1-\Phi}\right)$$

The stress level dependence of creep rate is described by a sinh function. Material parameters which appear in this model may be divided into three groups, i.e.

- the constants h, H^* which describe primary creep;
- the constants A and B which characterise secondary creep;
- the constants K_c and D responsible for damage evolution and failure.

The second equation in set (8.12) describes primary creep using variable H, which varies from 0 at the beginning of the creep process to H^*, where H^* is the saturation value of H at the end of primary period and subsequently maintains this value until failure.

The equation set contains two damage state variables used to model tertiary softening mechanisms:

- Φ, which is described by the third equation in set (8.12), is defined from physics of ageing to lie within the range 0–1 for mathematical convenience,
- ω_2, which is defined by the fourth equation in set (8.12), describes grain boundary creep constrained cavitation, the magnitude of which is strongly sensitive to alloy composition and the processing route.

The parameter N is used to indicate the state of loading; e.g. for σ_1 tensile $N = 1$; and for σ_1 compressive, $N = 0$. In the equation set (8.12) a damage evolution depends on the maximum principal stress as well as the effective stress. After appropriate integration of the normalised form of equation set (8.12) the isochronous surfaces can be achieved (Kowalewski et al. 1994). It has been shown that the shape of the isochronous rupture loci is independent of the damage level (ω_2) for which they are determined, but is dependent on the stress level. At lower stress levels the curves become more dependent on the maximum principal stress.

It has been found from the experimental investigations that the minimum creep rate, which is directly related to the primary creep controlled by $\dot{H}$ in equation set (8.12), varies with stress-states for both materials. In the second equation of set (8.12) $\dot{H}$ is only a function of σ_e and could not model the feature. In addition, the

rupture lifetime is not a constant of σ_1/σ_e for a given effective stress for both tested materials. This indicates that both the primary hardening and damage rate equations in (8.12) need to be modified. The modified equations are formulated based on set of equations (8.12) by taking into account the influence of stress-states on primary, secondary and tertiary creep. For the simplicity, only one damage state variable is used here to model grain boundary creep constrained cavitation. The evolutionary equations are given in the following form (Lin et al. 2005)

$$\begin{aligned}
\dot{\varepsilon}_e &= \frac{A}{(1-\omega)^n} \sinh\left(B\sigma_e(1-H)\right), \\
\dot{\varepsilon}_{ij} &= \frac{3}{2}\dot{\varepsilon}_e\left(\frac{\bar{S}_{ij}}{\sigma_e}\right), \\
\frac{dH}{dt} &= h(Q-H)\dot{\varepsilon}_e, \\
\frac{d\omega}{dt} &= D\left(\frac{\sigma_1}{\sigma_e}\right)^{\gamma} N\dot{\varepsilon}_e,
\end{aligned} \tag{8.13}$$

where $Q = Q_0(\sigma_1/\sigma_e)^{\phi}$ and $\gamma = \beta\sigma_1$. Parameter γ varies linearly with the maximum principal stress. The constant β is used to express the stress-state effects on the damage evolution of materials, and moreover, to model lifetimes and tertiary creep deformation behaviour of materials. Relation $\beta < 0$ indicates that the damage evolution of the material exceeds the effective stress control (a case typical for aluminium alloys), and, the presence of a low value of σ_1 would reduce the lifetime. If $\beta > 0$ then the damage evolution is under controlled by the effective stress. In the case of $\beta = 0$ the lifetime and tertiary creep of the material is controlled by effective stress only. The parameter N is introduced in (8.13) to ensure $\dot{\omega} = 0$, when σ_1 is compressive.

The evolution of the variable H in equation set (8.13) represents the primary hardening of the materials, which is mainly due to the accumulation of dislocation density during the primary creep process. As creep deformation proceeds, the increment of dislocation density and its recovery under elevated temperature reaches a dynamic balance condition. This is the steady-state, or, secondary creep, which is one of the most important properties in creep deformation. In the equation, the parameter Q, which indicates the end of primary creep and controls the secondary creep rate, is stress-state dependent and defined as $Q = Q_0(\sigma_1/\sigma_e)^{\phi}$. For the stress-state independent material, the constant $\phi = 0$ and $Q = Q_0$. Thus, Q is the saturation value of the primary hardening variable H and also determines the secondary creep rates, i.e. the minimum creep rate, $\dot{\varepsilon}_{min}$. However, if a material is stress-state dependent, $\phi \neq 0$, the value of Q varies with the ratio of the maximum principal stress and effective stress σ_1/σ_e. In consequence, the saturation value of the variable H changes with a variation of the stress-state. Thus, the minimum effective creep rates can be controlled according to the first equation of set (8.13). In this way, both primary and secondary creep periods are modelled by the introduction of the internal variable H.

The other material constants have the similar meanings as discussed for equation set (8.12). Optimisation techniques for the determination of the material constants arising in the constitutive equations are based on minimising the sum of the errors between the computed and experimental data using Evolutionary Algorithms (EA) (Lin and Yang 1999; Li et al. 2002). The fitness function used here for the optimisation based on the concept developed by Li et al. (2002). In this method, errors are defined by the shortest distance between computational and experimental data. An EA-based optimisation software package was developed using C++ based (Li et al. 2002). The multiaxial creep damage constitutive equations (equation set (8.13)) are implemented into the optimisation software package through a user-defined subroutine.

Figures 8.9 and 8.10 show the comparison of the experimental (symbols), and computed (solid curves) effective creep curves for the three stress-states for copper and aluminium alloy, respectively. The curves are computed using the determined material constants. It can be seen that there are some differences between the computed and experimental data, although the overall fitting quality is good. The difference might be due to the errors of the experimental results coming from always possible specimen-to-specimen variations of the material.

Presented here attempts for creep damage analysis reflect only advances in constitutive equations development in which the scalar damage measures are used. There are many papers devoted to creep damage where vector or tensor measures of damage were applied. Due to limits required for this chapter such issue is not discussed here.

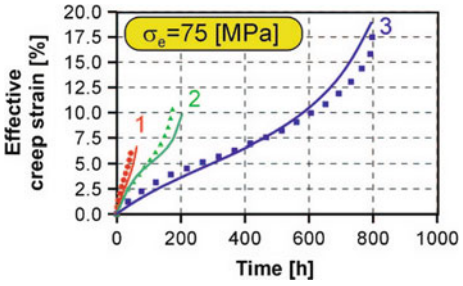

Fig. 8.9 Comparison of experimental and theoretical (equation set (8.13)) creep curves for pure copper at 423 K under stress equal to 75 MPa; *1* $(\sigma_{12}/\sigma_{11}) = 0$; *2* $(\sigma_{12}/\sigma_{11}) = \sqrt{3}/3$; *3* $(\sigma_{12}/\sigma_{11}) = \infty$

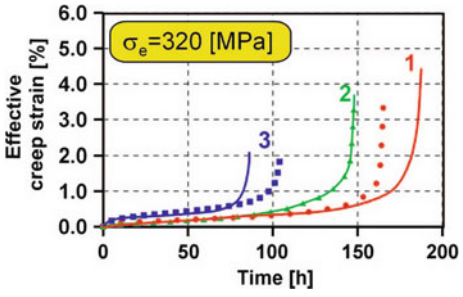

Fig. 8.10 Comparison of experimental and theoretical (equation set (8.13)) creep curves for pure copper at 423 K under stress equal to 320 MPa; *1* $(\sigma_{12}/\sigma_{11}) = 0$; *2* $(\sigma_{12}/\sigma_{11}) = \sqrt{3}/3$; *3* $(\sigma_{12}/\sigma_{11}) = \infty$

8.4 New Attempts for Damage Development During Creep

There are many testing techniques for creep damage analysis. They can be generally divided into destructive and non-destructive methods. To assess damage using destructive method the specimens after different amounts of prestraining were stretched to failure (Kowalewski et al. 2008, 2009; Makowska et al. 2014). Afterwards, the selected tension parameters were determined and their variations were used for identification of damage development. Ultrasonic and magnetic investigations were selected as the non-destructive methods for damage development evaluation. For the ultrasonic method, the acoustic birefringence coefficient was used to identify damage development in the tested steel. Two magnetic techniques for non-destructive testing were applied, i.e. measurement of the Barkhausen effect (HBE) and the magneto-acoustic emission (MAE). Both effects are due to an abrupt movement of the magnetic domain walls depicted from microstructural defects when the specimen is magnetised. The laboratory test specimens were magnetised by a solenoid and the magnetic flux generated in the specimen was closed by a C-core shaped yoke. The magnetizing current (delivered by a current source) had a triangular like waveform and frequency of order 0.1 Hz. Its intensity was proportional to the voltage Ug. Two sensors were used: (a) a pickup coil (PC), and (b) an acoustic emission transducer (AET). A voltage signal induced in the PC was used for the magnetic hysteresis loop $B(H)$ evaluation (low frequency component) as well as for the HBE analysis (high frequency component). The intensity of the HBE was given by the rms (root mean square) voltage Ub envelopes. The maximal values ($Ubpp$) of Ub for one period of magnetisation were compared. An analogous analysis was performed for the MAE voltage signal from the AET. In this case the maximal values ($Uapp$) of the Ua voltage envelopes were compared. The magnetic coercivity Hc, evaluated from the $B(H)$ hysteresis loop plots, was also compared.

8.4.1 Experimental Details

The X10CrMoVNb9-1 steel commonly used in selected elements of Polish power plants was investigated. Its chemical composition is presented in Table 8.2.

The experimental programme comprised tests for the material in the as-received state and for the same material subjected to a range of selected magnitudes of prior deformation due to creep at elevated temperatures, Fig. 8.11, and due to plastic flow at room temperature, Fig. 8.12. Uniaxial tension creep tests were carried out for the

Table 8.2 Chemical composition of the X10CrMoVNb9-1 steel

C	Mn	Nb	P	S	Cr	Ni	Mo	V	Cu
0.10	0.70	0.07	0.01	0.01	8.50	0.30	0.94	0.22	0.20

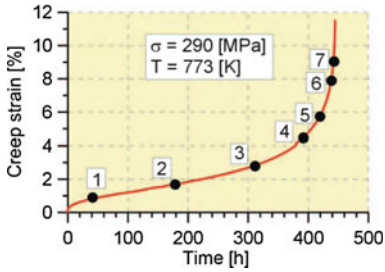

Fig. 8.11 Creep curve of X10CrMoVNb9-1 steel with points representing interrupted creep tests

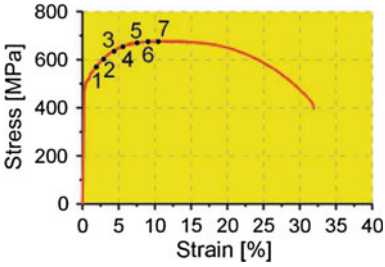

Fig. 8.12 Tension curve of X10CrMoVNb9-1 steel with points representing interrupted tensile tests

X10CrMoVNb9-1 steel using plane specimens, Fig. 8.13. All tests were conducted in the same conditions: i.e. the stress level was 290 MPa, and the temperature was 773 K. Details of the destructive tests programme as well as its main results are presented by Kowalewski et al. (2008).

In order to assess damage development during creep the tests for the X10CrMoVNb9-1 steel were interrupted after 40 h (0.85 %), 180 h (1.85 %), 310 h (3.15 %), 390 h (4.6 %), 425 h (5.9 %), 440 h (7.9 %) and 445 h (9.3 %), which correspond to increasing amounts of creep strain (values are presented in brackets). To check how deformation type changes damage development, almost the same prestraining levels as those under creep were induced by means of plastic flow: 2, 3, 4.5, 5.5, 7.5, 9, and 10.5 %, Fig. 8.12. After each prestraining test the specimen damage was assessed using the non-destructive methods. Two non-destructive methods were applied: magnetic (Augustyniak 2003) and ultrasonic (Szelążek 2001). In the next step of the experimental procedure, the same specimens were mounted on a hydraulic servo-controlled MTS testing machine and then stretched until failure was achieved.

8.4.1.1 Non-destructive Techniques

Magnetic properties were measured using the standard laboratory method of magnetisation, where hysteresis loops with the HBE and also the MAE can be tested (Augustyniak 2003; Augustyniak et al. 2000). A block diagram of the magnetising circuit is shown in Fig. 8.14. A specimen (1) was magnetised with the driving coil (2). A current amplifier provided a triangular wave-form with a frequency of about

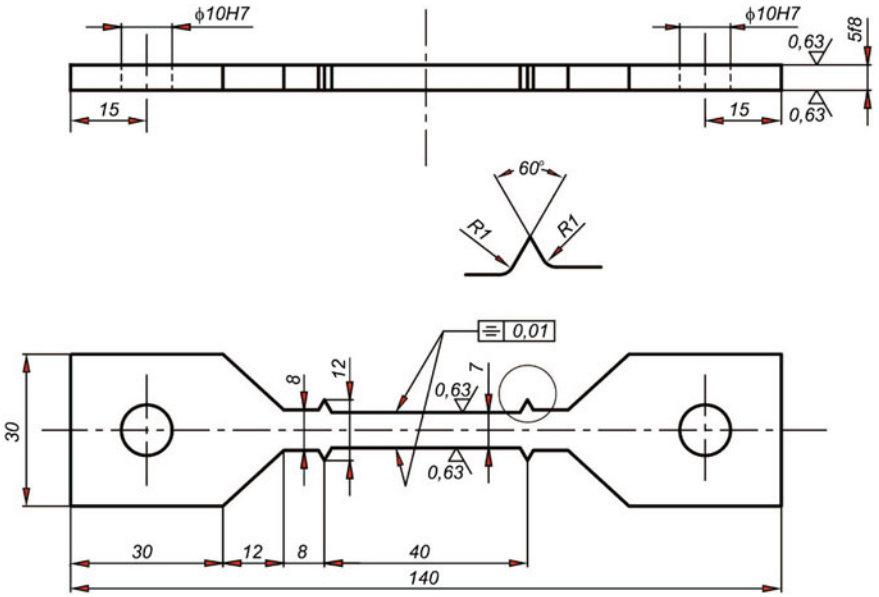

Fig. 8.13 Specimen for creep and plastic f low tests

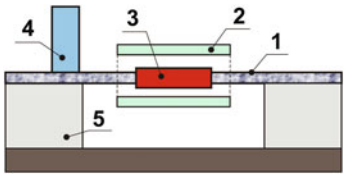

Fig. 8.14 Measuring set for magnetic properties: *1* specimen, *2* driving coil, *3* pick-up coil, *4* MAE detector, *5* magnetic core (Augustyniak 2003)

1 Hz. Magnetic measurements were made with a pickup coil of 200 turns wound directly on the central part of the specimen. The voltage U induced in this coil was used to determine the hysteresis loop and the HBE signal. The HBE signal was separated from the U signal using an ac amplifier. The output voltage was transformed to the rms like voltage Ub (intensity envelope). This envelope of the HBE intensity is presented when the HBE envelopes are compared. The MAE signal was detected with a resonant PZT transducer. The output of the MAE voltage signal was amplified and then transformed to the Ua voltage using the analogous rms integral circuit.

The HBE properties along the specimen were also investigated as well as the relationships between the HBE and static load by means of bending. Figure 8.15 illustrates the experimental setup used for measurement of the HBE stress dependence. Here, the HBE intensity was measured not at the specimen central part, but near the specimen end. Each specimen was loaded by means of bending. A probe during the HBE tests contains ferrite with a pick-up coil. The probe was used for the HBE intensity measurement along the specimen. It was connected to the MEB-1

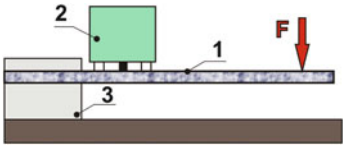

Fig. 8.15 Measuring set for stress dependence of HBE: *1* specimen, *2* HBE probe, *3* metal support, *F* applied force (Augustyniak 2003)

meter. This meter provides not only an analog rms voltage, but also a signal proportional to the pulse counting rate and total number of detected pulses (Nc) with amplitudes higher than a certain threshold level.

Ultrasonic wave velocity and attenuation are acoustic parameters most often used to assess material damage due to creep or fatigue. The results of investigations (Fel et al. 2001; Martínez-Ona and Pérez 2000) show that the attenuation of ultrasonic waves is in practice stable until the last creep or fatigue stages. It was also observed that velocity changes due to creep or fatigue are small, and therefore, an application of velocity measurement for damage evaluation, in industrial conditions, is very difficult. Difficulties in the attenuation and velocity measurements, or their combinations, are caused by the heterogeneous acoustic properties of technical materials, such as steel. The second reason is a dependence of both the attenuation and velocity of ultrasonic waves on numerous factors other than material damage. This observation is confirmed by the results of tests (Martínez-Ona and Pérez 2000) where the steel specimens were subjected to 10 % plastic deformation and subjected to loading for a period of 140,000 h at elevated temperature. The results showed that the ultrasonic wave attenuation was not influenced by the plastic deformation or long term, high temperature load exposure.

In order to evaluate damage progress in specimens made of X10CrMoVNb9-1 steel, instead of the velocity and attenuation measurement, the acoustic birefringence B was measured (Kowalewski et al. 2008, 2009). Specimens were subjected to creep according to the programme presented earlier in this paper.

The acoustic birefringence B is a measure of material acoustic anisotropy. It is based on the velocity difference of two shear waves polarized in the perpendicular directions. In specimens subjected to creep the shear waves were propagated in the specimen thickness direction and were polarized along its axis and in the perpendicular direction. The birefringence was measured in the fixtures, where a texture of material was assumed to be unchanged during a creep test, and in the working part of the specimen, Fig. 8.16. The birefringence B was calculated using the following expression (Szelążek 2001):

$$B = \frac{2(t_l - t_p)}{t_l + t_p} = B_0 + B_P \tag{8.14}$$

where: t_l—time of flight of ultrasonic shear wave pulse for the wave polarization direction parallel to the sample axis, t_p—time of flight of ultrasonic shear wave

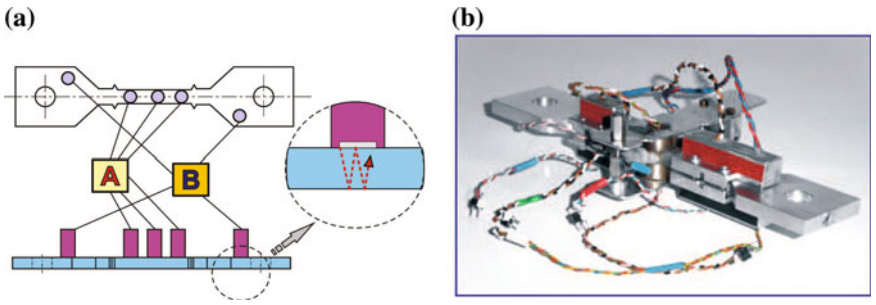

Fig. 8.16 Set-up for measurements of the birefringence coefficient: **a** scheme showing positions of probes (*B* probes at the griping part of specimen, *A* probes distributed along gauge length of specimen); **b** general view of specimen before ultrasonic testing

pulse for the wave polarization perpendicular to the sample axis, B_0—acoustic birefringence for the material in the virgin state (before creep test), B_P—acoustic birefringence for the material after deformation.

8.4.2 Experimental Results and Discussion

8.4.2.1 Evaluation of Damage Development Using Destructive Tests

The tensile characteristics for the material after prestraining are presented in Fig. 8.17. In diagrams the characteristics for the prestrained steel are compared to the tensile curve of steel in the as-received state.

On the basis of these tensile characteristics, Fig. 8.17, variations of the basic mechanical properties of steel, due to deformation achieved by prior creep or plas-

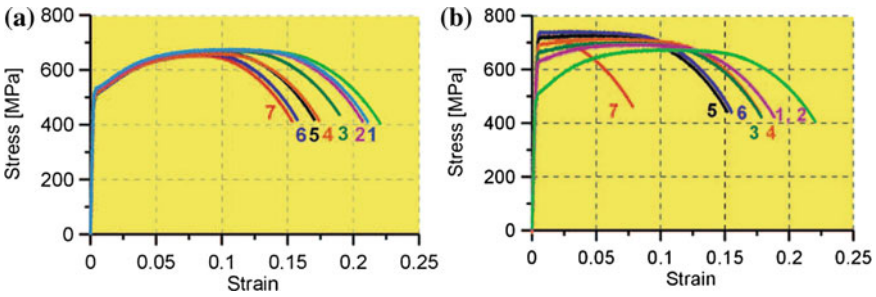

Fig. 8.17 Tensile characteristics of the X10CrMoVNb9-1 steel: **a** material after prior deformation due to creep interrupted in different phases of damage development, **b** material after prior deformation due to plastic flow interrupted in different phases of the process, (numbers correspond to those in Figs. 8.11 and 8.12 presented)

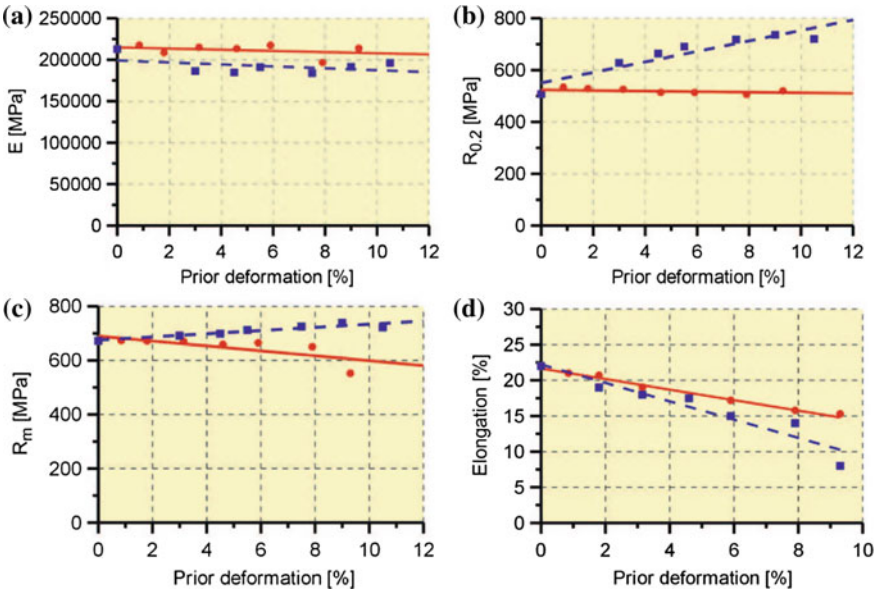

Fig. 8.18 Variation of tensile parameters of the X10CrMoVNb9-1 steel due to creep (*solid lines*) and plastic (*broken lines*) deformations: **a** Young's modulus; **b** yield point; **c** ultimate tensile strength; **d** elongation

tic flow were determined, Fig. 8.18. It was observed that the Young's modulus, Fig. 8.18a, is almost insensitive to the magnitude of creep and plastic deformations.

Contrary to the Young's modulus the other considered tension test parameters, especially the yield point, Fig. 8.18b, and the ultimate tensile strength, Fig. 8.18c, exhibit clear dependence on the level of prestraining. Taking into account the results presented for the steel a difference between magnitudes of such parameters as the yield point or ultimate tensile strength observed for the same value of prior deformation induced by creep and plastic flow is quite significant. Prior plastic deformation caused the hardening of the steel, while creep prestraining led to its softening. It is important to note that the observed softening effect is only expressed on the basis of the ultimate tensile strength variations since for the testing conditions applied in these investigations the magnitude of the yield point is not sensitive to the amount of prior creep deformation.

8.4.2.2 Evaluation of Damage Development Using Magnetic Techniques

An influence of plastic flow and creep damage on the basic magnetic properties can be analysed using $B(H)$ hysteresis loops. Representative results are presented in Figs. 8.19 and 8.20 for the X10CrMoVNb9-1 steel. The curves obtained for an undamaged specimen ($\varepsilon = 0\,\%$) and for the specimens after prior deformation are

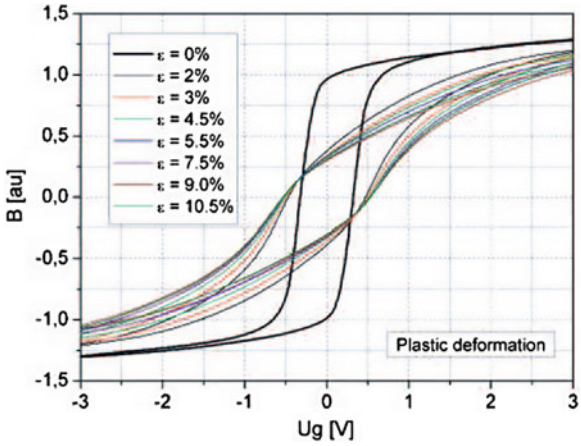

Fig. 8.19 Evaluated magnetic hysteresis loops of undamaged and damaged specimens due to plastic flow

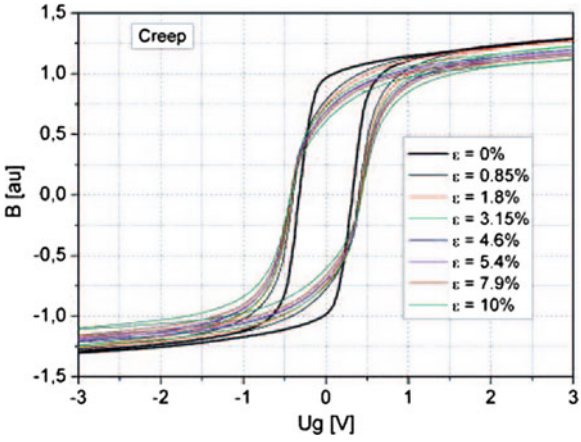

Fig. 8.20 Evaluated magnetic hysteresis loops of undamaged and damaged specimens due to creep

compared. The quantity Ug denotes the voltage proportional to the driving current intensity, and hence—magnetic field strength H.

The broadening as well as the decrease of the slope of the $B(H)$ loops for both cases is evident. Taking into account the same prestrain levels the effects are much more intensive in the case of plastic flow than those after creep. The coercivity Hc was evaluated from the width of $B(Ug)$ plot at $B = 0$, Fig. 8.21. The observed systematic increase of coercivity is due to an increase of pining force of the 180° magnetic domain walls by damage induced modifications of microstructure. It should be emphasised that there is a two times higher increase of the coercivity (about $+60\,\%$) for the specimens after plastic flow than for the specimens after creep (about $+30\,\%$).

Modification of the hysteresis properties, as shown by the HBE intensity envelopes, can be deduced from the series of plots presented in Figs. 8.22 and 8.23 for specimens

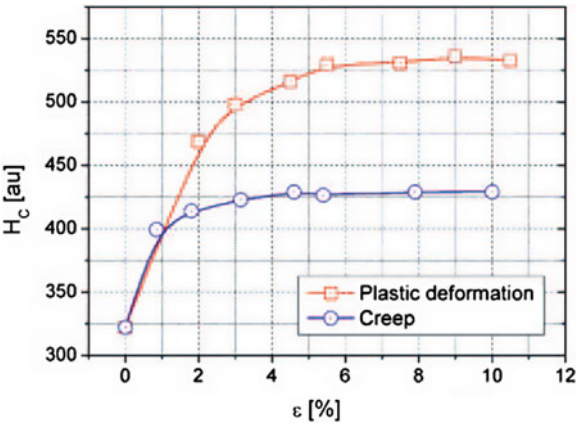

Fig. 8.21 Dependence between the coercivity and deformation for specimens after plastic flow (*squares*) and after creep (*circles*)

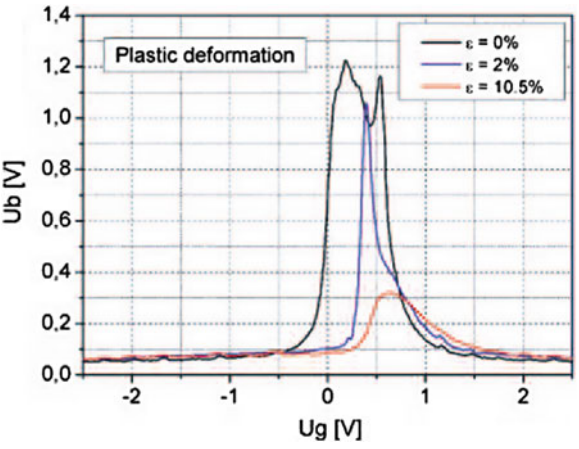

Fig. 8.22 Envelopes of the HBE intensity in function of increasing field strength for the undamaged specimen ($\varepsilon = 0$) and for two specimens after plastic flow

after plastic flow and after creep, respectively. It has to be noticed that there is an increase of the scale of the Ub values in Fig. 8.23. Such a presentation of the results was made in order to show the very high increase of the HBE intensity after the first step of the creep damage experiment in comparison to the initial stage signal. The HBE intensity envelope for an undamaged sample is characterised by a shape consisting of two peaks. The X10CrMoVNb9-1 steel has a martensitic microstructure, and thus, the first peak (positioned at lower field strength) can be attributed formally to the 'soft' component of the alloy while the second one to the 'hard' component without detailed discussion about the microstructure reference, which can be done after microscopic inspection of the magnetic domain structure.

The increase of the plastic strain after plastic flow leads to some general decrease of the HBE intensity: for the first tested stage of deformation ($\varepsilon = 2\,\%$) one narrow peak appears and further plastic flow leads to a monotonic decrease of its amplitude as well as to the decrease of the area under the signal envelope. A shift of the

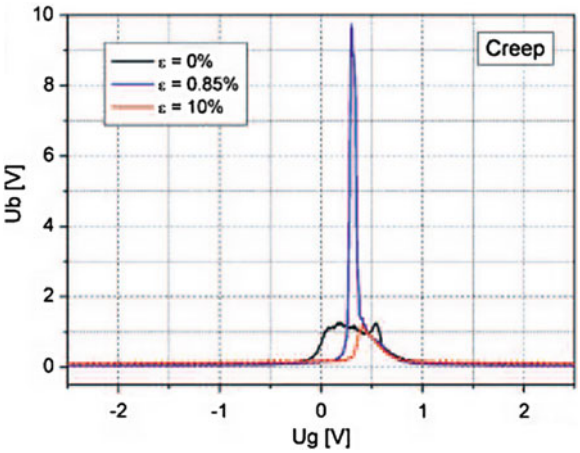

Fig. 8.23 Envelopes of the HBE intensity in function of increasing field strength for the undamaged specimen (1) ($\varepsilon = 0$) and for two specimens after creep damage

maximum towards a higher level of the magnetic field strength can also be clearly seen. However, the behaviour of the Ub properties when the samples are subjected to creep damage is very different. Figure 8.23 shows that for a low level of creep damage ($\varepsilon = 0.85\,\%$) the plot of the Ub envelope appears as one very high, narrow peak. Such behaviour can be explained by the increase of the 180° domain walls mobility due to the decrease of internal stress level resulting from an annealing or—more probably, by anisotropy of magnetic domain structure due to the tensile load applied, enhanced by the high temperature. Further creep damage leads to the systematic decrease of this peak amplitude as well as to its shift toward higher field strength.

The as described features of the HBE intensity are well presented by means of plots showing a dependence between the amplitudes of Ub envelopes and magnitudes of prior deformation—peak to peak values Ub_{pp} in Fig. 8.24, and a dependence between the integrals of the Ub envelopes and prior deformation (Fig. 8.25) for specimens after plastic flow (squares) and after creep (circles). Thus, one can say that the HBE intensity as a function of the resulting prestrain either decreases monotonically (for integrals) or peaks when amplitudes of the Ub envelopes are compared. These two sets of plots reveal also that creep damage leads (at its final stage) to a 'decrease' of the HBE intensity which is much lower than that observed for specimens after plastic flow. Comparing two plots in each figure it can be seen that the Ub signal properties such as the amplitude or integral for the highest strain after creep damage are roughly the same as for the analogous signals for the first stage of plastic flow.

The main features of the magnetoacoustic effect are shown in Fig. 8.26 (after plastic flow) and in Fig. 8.27 (after creep).

The MAE intensity envelope for undamaged specimens is also characterised by the existence of two peaks. Comparing plots in Figs. 8.22 and 8.26 one can easily check that the plot of the MAE intensity envelope (Ua) is much broader than the plot of the Ub intensity. It is due to the fact that the MAE is caused mainly by an abrupt movement of 'not' 180° domain walls. The first peak is usually attributed mainly

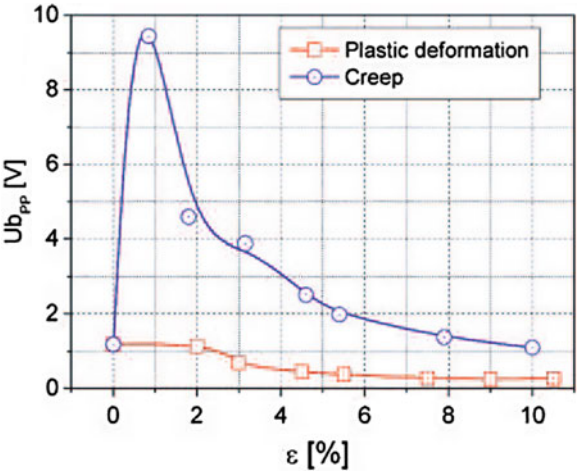

Fig. 8.24 Dependence between the amplitudes of Ub envelopes and deformation for specimens after plastic flow (*squares*) and after creep (*circles*)

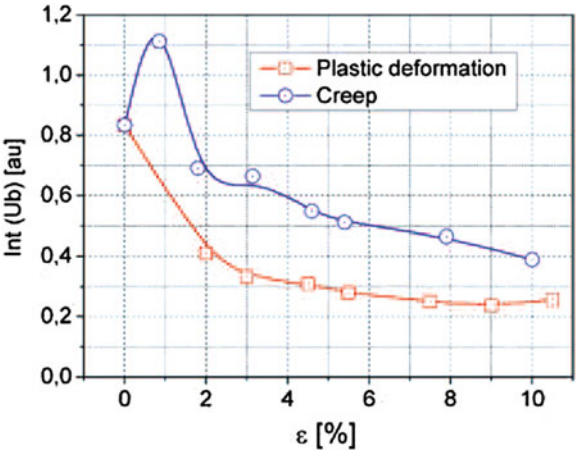

Fig. 8.25 Dependence between the integrals of Ub envelopes and deformation for specimens after plastic flow (*squares*) and after creep (*circles*)

to a creation of the magnetic domains, and the second one—to their annihilation. Both processes are characterised by a high contribution of this type of domain walls (Augustyniak et al. 2000). These pictures also show that plastic flow as well as creep damage modifies the MAE intensity significantly.

The plastic flow modifies the MAE intensity in two ways: the two peaks observed after the first step of flow ($\varepsilon = 2\,\%$) are broader and their amplitudes are much smaller. This means that the produced dislocations tangles have strongly blocked the mobility of 'not' 180° domain walls. Further plastic flow leads to a monotonic decrease of the MAE intensity.

Again, the results of creep damage show an influence of prior deformation on the MAE properties, as shown by the plots in Fig. 8.27. The stage with small creep deformation level ($\varepsilon = 0,85\,\%$) is characterised by a single, narrow peak. This

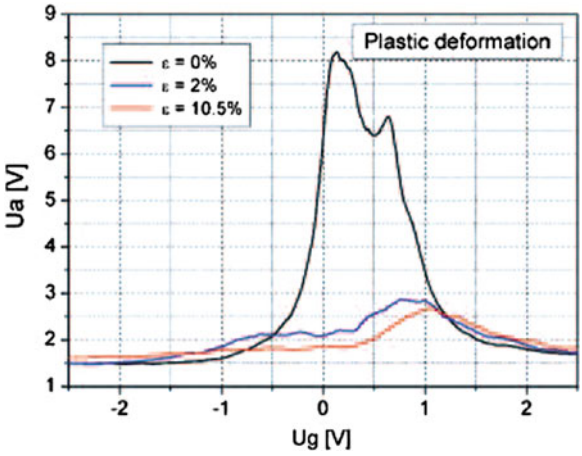

Fig. 8.26 Envelopes of the MAE intensity as a function of increasing field strength for the undamaged specimen (plot 1, $\varepsilon = 0$) and for two specimens after plastic flow

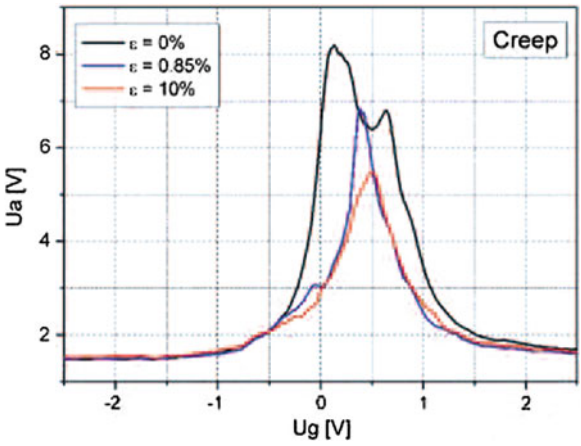

Fig. 8.27 Envelopes of the MAE intensity as a function of increasing field strength for the undamaged specimen (plot 1, $\varepsilon = 0$) and for two specimens after creep damage

means that now the displacement of 'not' 180° domain walls may become the main contributor to the MAE instead of the creation and annihilation processes. A synthetic description of the MAE properties as a function of prior deformation is given by the two sets of plots shown in Fig. 8.28 (amplitudes of the MAE envelopes) and in Fig. 8.29 (integrals of the MAE envelopes). Amplitudes of the MAE intensity decrease for both cases, but the dynamics of their change is different, as is evident from Fig. 8.28. Moreover, amplitudes of the MAE intensity envelopes do not decrease so abruptly for the creep prestrained specimens, and do not reach the level obtained for the first step of plastic deformation due to plastic flow at room temperature.

Figure 8.29 shows how integrals of the MAE intensity vary with the increasing prior deformation. The dynamic of the integrals decrease is not as high as that observed in the case of amplitudes. However, a difference between both types of damage is still visible. It is easy to observe that a level of the MAE intensity (esti-

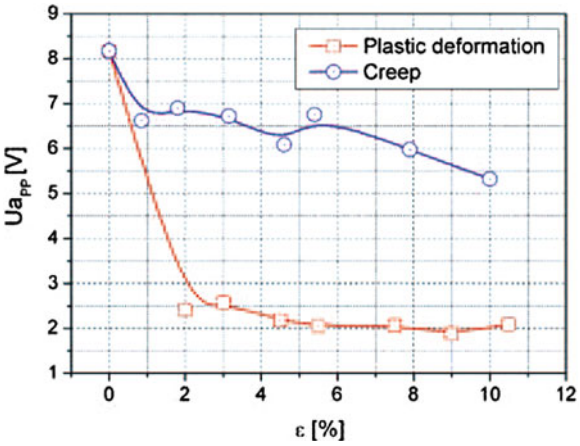

Fig. 8.28 Dependence between amplitudes of Ua envelopes and prior deformation due to plastic flow (*squares*) and creep (*circles*)

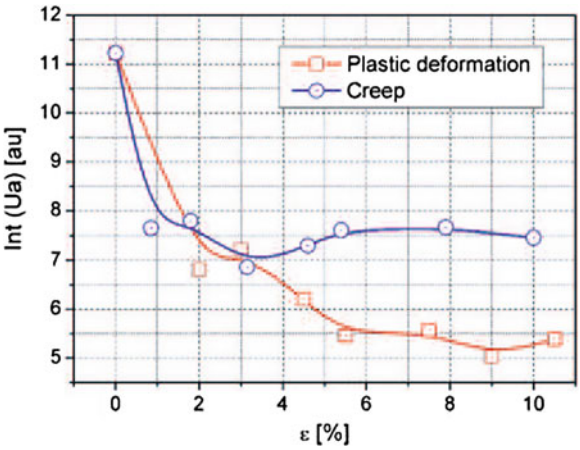

Fig. 8.29 Dependence between integrals of Ua envelopes and prior deformation due to plastic flow (*squares*) and creep (*circles*)

mated by means of the integral) for the specimen after creep with a strain of order $\varepsilon = 10\,\%$ is nearly the same as that detected for specimens after plastic deformation with a strain level of order $\varepsilon = 2\,\%$. However, it does not mean that these two specimens have the same microstructure. A difference in the microstructure for these two stages is demonstrated well by different shapes of the Ua envelopes for $\varepsilon = 2\,\%$ (Fig. 8.26) and for $\varepsilon = 10\,\%$ (Fig. 8.27). The stresses which influence the MAE activity are located inside the cells made by dislocation tangles. They are 'created' by these tangles and can be highly compressive in the case of plastic deformation. The MAE intensity is also influenced by the precipitates developing mainly at grain boundaries.

8.4.2.3 Evaluation of Damage Development Using Ultrasonic Technique and Correlations of Damage Sensitive Parameters

Figure 8.30 presents mean values of the acoustic birefringence measured in specimens after creep or plastic deformation.

The birefringence was measured in the fixtures, where the texture of the material was assumed to be unchanged during creep testing, and in the working part of the specimen. The plots presented in Fig. 8.30 indicate that the acoustic birefringence is sensitive to the amount of prior deformation. Another advantage of this parameter is also well represented in Fig. 8.30. Namely, it is sensitive to the form of prior deformation. For specimens prestrained due to plastic flow a decrease of this parameter is observed with the increase of prior deformation. In the case of prior creep also decrease of acoustic birefringence is observed, however, it is not as large as that after plastic deformation obtained. The results show that the acoustic birefringence can be a quite sensitive indicator of material degradation and can help to locate the regions where material properties are changed due to creep. Measurements of the ultrasonic wave attenuation and velocities carried out on the same steel did not exhibit such a good sensitivity in the material damage assessments.

In the next step of analysis possible relations between the mechanical and magnetic parameters were evaluated Figs. 8.31, 8.32, 8.33, 8.34 and 8.35.

Figures 8.31, 8.32, 8.33 and 8.34 show relationships between two magnetic parameters of MBE: i.e. Ub_{pp} and Int(U_b) and two mechanical parameters: i.e. yield point and ultimate tensile strength. Figures 8.31 and 8.32 do not include results of

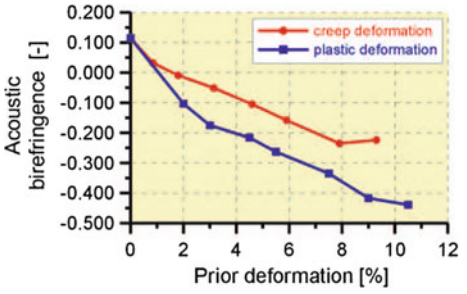

Fig. 8.30 Acoustic birefringence B variations due to prior deformation of the X10CrMoVNb9-1 steel

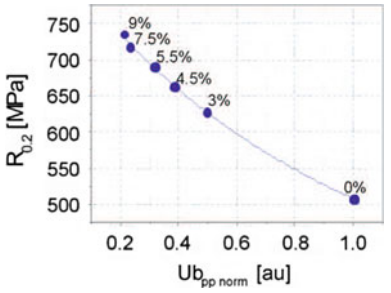

Fig. 8.31 Variation of yield point of the X10CrMoVNb9-1 steel versus amplitude of the magnetic Barkhausen emission (results for steel prestrained due to plastic flow)

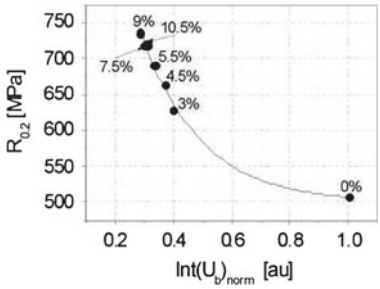

Fig. 8.32 Variation of yield point of the X10CrMoVNb9-1 steel versus integral over half-period voltage signal of the magnetic Barkhausen emission (results for steel prestrained due to plastic flow)

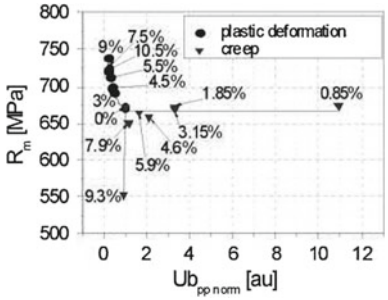

Fig. 8.33 Variation of ultimate tensile stress of the X10CrMoVNb9-1 steel versus amplitude of the magnetic Barkhausen emission

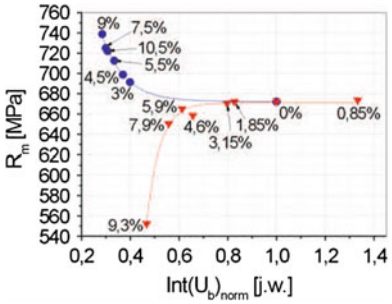

Fig. 8.34 Variation of ultimate tensile stress of the X10CrMoVNb9-1 steel versus integral over half-period voltage signal of the magnetic Barkhausen emission (*triangles* steel after creep; *circles* steel after plastic flow)

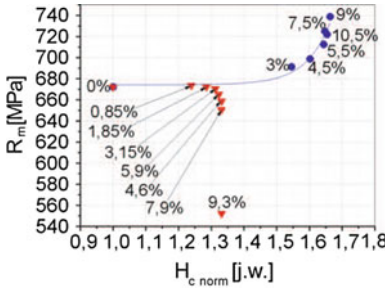

Fig. 8.35 Variation of ultimate tensile stress of the X10CrMoVNb9-1 steel versus coercivity (*triangles* steel after creep; *circles* steel after plastic flow)

the material prestrained due to creep, since the yield point of the X10CrMoVNb9-1 steel subjected to creep was insensitive to deformation level induced by this process. The magnetic parameters are normalized to values captured for the non-deformed specimen. Numbers in figures denote the level of prior deformation. Figures 8.31 and 8.32 allow concluding that both parameters (Ub_{pp} and Int(U_b)) of the Barkhausen noise may be used to estimate a level of the yield point of plastically deformed specimens. Also, the ultimate tensile strength of the X10CrMoVNb9-1 steel subjected to prior plastic flow may be assessed using relationships between R_{m} and $Ub_{pp\,\mathrm{norm}}$ or $\mathrm{Int}(Ub)_{\mathrm{norm}}$ (Figs. 8.33 and 8.34), however, only for the material prestrained due to plastic flow, since non-unique relationships between R_{m} and $Ub_{pp\,\mathrm{norm}}$ or $\mathrm{Int}(Ub)_{\mathrm{norm}}$ were found for the steel pre-strained by creep.

The relations in Figs. 8.31, 8.32, 8.33 and 8.34 indicate that the steel after plastic deformation, leading to higher values of $R_{0.2}$ and R_{m}, can be characterised by lower values of magnetic parameters. This is because the prestrained material contains more dislocation tangles that impede domain walls movement. On the other hand the higher values of magnetic parameters can be attributed to the lower magnitudes of R_{m} for the steel after creep.

The results make evident that the MBE intensity varies significantly due to microstructure modification, however, in different ways depending on prior deformation type. This intensity decreases after plastic flow (for deformation higher than 2 %) and increases after creep. Strongly non-linear character of plots in Figs. 8.33 and 8.34 makes impossible direct estimation of mechanical parameters when only single magnetic parameter is used. Addressing the issue for practical application of the MBE measurement in assessment of mechanical properties for damaged steel one can conclude that it is possible only then if at least two magnetic parameters will be taken into account. It can be seen in Figs. 8.33 and 8.34 that relative decrease of the Ub_{pp} and Int(U_b) with prestraining denotes plastic deformation while rapid increase of the Int(U_b) associated with prestrain increase is observed for early stage of creep damage development. The most difficult case for interpretation takes place when advanced creep is in question. It should be emphasized that such analysis can be done by simultaneous analysis of plots in Figs. 8.33 and 8.34 and the MBE peak shape variations. The results obtained for such case are not consistent, i.e. points representing subsequent magnitudes of prior deformation are not placed in order, and therefore, cannot be described be an adequate function.

Better correlation was achieved between R_{m} and coercivity H_{c}, Fig. 8.35. As it is seen, except specimen prestrained up to 10.5 % due to plastic flow, all results are ordered, and as a consequence, they can be well described by adequate functions depending on the type of prior deformation. The main disadvantage of the relationships between R_{m} and H_{c}, is related to the fact that it cannot distinguish a type of prior deformation for small prestrain magnitudes.

Similar remarks can be formulated for the relationships between R_{m} and acoustic birefringence coefficient B, Fig. 8.36.

The relationships between selected destructive and non-destructive parameters sensitive for damage development show a new feature that may improve damage identification. In order to provide more thorough analysis reflecting physical

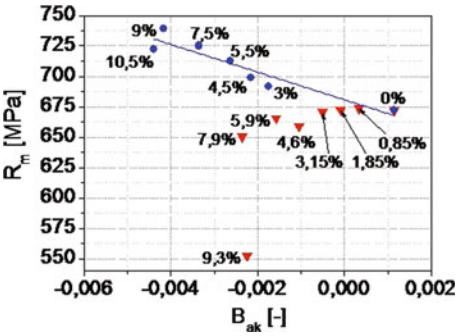

Fig. 8.36 Variation of ultimate tensile strength of the X10CrMoVNb9-1 steel versus acoustic birefringence (*triangles* steel after creep; *circles* steel after plastic flow)

interpretation of the relationships obtained further investigations are necessary. Programmes of such tests should contain advanced microscopic observations using not only optical techniques, but also SEM and TEM.

8.5 Concluding Remarks

This chapter is devoted to creep analysis using selected experimental methods. A short survey dealing with theoretical aspects of creep investigations is also presented.

It is shown that prior plastic deformation changes significantly values of the typical creep parameters. Depending of the magnitude of prestraining some of these parameters can be improved, the others however, become to be weaker than those for the nonprestrained material achieved. The tensile creep resistance measured as the value of steady creep rate was generally enhanced by plastic prestrain, which was expressed by significant decrease of the steady creep rate. The effect has proportional character up to certain limit value of plastic deformation, only. The creep data for aluminium alloy exhibit essential lifetime variation due to prestraining in both temperatures in question (423 and 473 K), namely, an extension of lifetime proportional to the magnitude of plastic prestrain. It has to be noted however, that plastic prestrain magnitudes greater than 6 % led to the opposite effect, i.e. lifetime reduction. The amount of creep deformation for both temperatures considered was markedly reduced by prior tensile plastic strain, yielding very low levels. Elongation of the testpieces was proportionally decreased when the magnitude of plastic prestrain was increased.

The chapter emphasises significance of the multiaxial creep testing, and identifies procedures for elaboration of data captured from such investigations.

This study also presents the results of interdisciplinary tests for damage assessments as a new promising tool for damage identification.

It is shown that the same level of deformation induced due to different processes does not guarantee the same mechanical properties of a material.

The results clearly indicate that selected ultrasonic and magnetic parameters can be good indicators of material degradation and can help to locate the regions where material properties are changed due to prestraining. In order to evaluate damage progress in specimens made of the X10CrMoVNb9-1 steel, instead of velocity and attenuation measurements frequently applied, the acoustic birefringence B measurements were successfully applied. In the case of magnetic investigations for damage identification the measurements of the Barkhausen effect (HBE) and the magneto-acoustic emission (MAE) were applied. Both effects show that the magnetic properties are highly influenced by prior deformation, and moreover, they are sensitive not only to the magnitude of prior deformation, but also to the way it is introduced.

The results suggest that experimental investigations concerning creep problems should be based on the interdisciplinary tests giving a chance to find mutual correlations between parameters assessed by classical macroscopic destructive investigations and parameters coming from the non-destructive experiments. Such relationships should be supported by thorough microscopic tests, thus giving more complete understanding of the phenomena observed during creep damage development.

References

Abo El Ata MM, Finnie I (1972) On the prediction of creep-rupture life of components under multiaxial stress. In: Hult J (ed) Proceedings of IUTAM symposium on creep in structures 1970, Gothenburg. Springer, Berlin, pp 80–95

Ashby MF, Gandhi C, Taplin DMR (1979) Fracture-mechanism maps and their construction for f.c.c. metals and alloys. Acta Metallurgica 27:699–729

Augustyniak B (2003) Magnetoelastic effects and their application in the non-destructive testing of materials (in Polish). Publishing House of Gdańsk University of Technology, Gdańsk

Augustyniak B, Chmielewski M, Sablik MJ (2000) Multiparameter magnetomechanical NDE. IEEE Trans Magn 36(5):3624–3626

Browne RJ, Lonsdale D, Flewitt PEJ (1981) The role of stress state on the creep rupture of 1%Cr1/2%Mo and 12%Cr1%MoVW tube steels. In: Wilshire B, Owen D (eds) Creep and fracture of engineering materials and structures. Pineridge Press, Swansea, pp 545–557

Chrzanowski M, Madej J (1980) The construction of failure limit curves by means of a damage. J Theor Appl Mech 18:587–601 (in Polish)

Dietrich L, Kowalewski ZL (1997) Experimental investigation of an anisotropy in copper subjected to predeformation due to constant and monotonic loadings. Int J Plast 13:87–109

Dyson BF, Gibbons TB (1987) Tertiary creep in nickel-base superalloys: analysis of experimental data and theoretical synthesis. Acta Metallurgica 35:2355–2369

Dyson BF, McLean D (1977) Creep of nimonic 80A in torsion and tension. Metal Sci 11:37–45

Dyson BF, Rodgers MJ (1974) Prestrain, cavitation and creep ductility. Metal Sci 8:261–266

Dyson BF, Loveday MS, Rodgers MJ (1976) Grain boundary cavitation under various states of applied stress. Proc R Soc Lond A349:245–259

Fel D, Hsu DK, Warchol M (2001) Simultaneous velocity, thickness and profile imaging by ultrasonic scan. J Nondest Eval 8:95–112

Garofalo F (1965) Fundamentals of creep and creep rupture in metals. Macmillan, New York

Gittus J (1975) Creep. Viscoelasticity and creep fracture in solids. Wiley, New York

Hayhurst D, Trąmpczyński WA, Leckie FA (1980) Creep rupture under non-proportional loading. Acta Metallurgica 28:1171–1183

Hayhurst DR (1972) Creep rupture under multi-axial states of stress. J Mech Phys Solids 20:381–390
Hayhurst DR (1983) On the role of creep continuum damage in structural mechanics. In: Wilshire B, Owen D (eds) Engineering approaches to high temperature design. Pineridge Press, Swansea, pp 85–176
Johnson AE, Henderson J, Mathur VD (1956) Combined stress fracture of commercial copper at 250 C. The Eng 202:261
Johnson AE, Henderson J, Khan B (1962) Complex-stress creep. Relaxation and fracture of metallic alloys. H.M.S.O, Edinburgh
Kachanov LM (1958) The theory of creep (English Translation Edited by Kennedy AJ). National Lending Library, Boston Spa
Kowalewski Z (1991a) Creep behavior of copper under plane stress state. Int J Plast 7:387–404
Kowalewski Z (1991b) The influence of deformation history on creep of pure copper. In: Życzkowski M (ed) Creep in structures. Springer, Berlin, pp 115–122
Kowalewski ZL (1992) The role of grain size on creep of copper under uniaxial tension. Arch Metall 37:65–76
Kowalewski ZL (1995) Experimental evaluation of the influence of stress state type on creep characteristics of copper at 523K. Arch Mech 47:13–26
Kowalewski ZL (1996) Biaxial creep study of copper on the basis of isochronous creep surfaces. Arch Mech 48:89–109
Kowalewski ZL (2002) Creep rupture analysis of metals under complex stress state. In: Skrzypek J, Ganczarski A (eds) Anisotropic behaviour of damaged materials. Springer, Kraków-Przegorzały, pp 79–92
Kowalewski ZL (2004) Isochronous creep rupture loci for metals under biaxial stress. J Strain Anal Eng Des 39:581–593
Kowalewski ZL (2005) Creep analysis of M1E copper and PA6 aluminium alloy subjected to prior plastic deformation. J Theor Appl Mech 43:241–256
Kowalewski ZL, Hayhurst DR, Dyson BF (1994) Mechanisms-based creep constitutive equations for an aluminium alloy. J Strain Anal 29:309–316
Kowalewski ZL, Szelążek J, Mackiewicz S, Pietrzak K, Augustyniak B (2008) Evaluation of damage in steels subjected to exploitation loading—destructive and non-destructive methods. Int J Modern Phys Lett B 22:5533–5538
Kowalewski ZL, Szelążek J, Mackiewicz S, Pietrzak K, Augustyniak B (2009) Evaluation of damage development in steels subjected to exploitation loading—destructive and nondestructive techniques. J Multiscale Model 1:479–499
Krauss G (1996) Fatigue and fracture. In: ASM Handbook. ASM International, OH, pp 680–690
Leckie FA, Hayhurst DR (1977) Constitutive equations for creep rupture. Acta Metallurgica 25:1059–1070
Li B, Lin J, Yao X (2002) A novel evolutionary algorithm for determining unified creep damage constitutive equations. Int J Mech Sci 44:987–1002
Lin J (2003) Damage mechanisms, models and calibration techniques. In: Dietrich L (ed) Training course on mechanics—Proceedings of mechanical investigations of material properties and structures. IPPT PAN, Warszawa, pp 123–143
Lin J, Yang J (1999) GA based multiple objective optimization for determining viscoplastic constitutive equations for superplastic alloys. Int J Plast 15:1181–1196
Lin J, Kowalewski ZL, Cao J (2005) Creep rupture of copper and aluminium alloy under combined loadings—experiments and their various descriptions. Int J Mech Sci 47:1038–1058
Litewka A, Hult J (1989) One parameter CDM model for creep rupture prediction. Eur J Mech A/Solids 8:185–200
Makowska K, Kowalewski ZL, Augustyniak B, Piotrowski L (2014) Determination of mechanical properties of P91 steel by means of magnetic Barkhausen emission. J Theor Appl Mech 52:181–188
Malinin N, Rżysko J (1981) Mechanics of materials. PWN, Warszawa (in Polish)

Marlin RT, Cosandey F, Tien JK (1980) The effect of predeformation on the creep and stress rupture of an oxide dispersion strengthened mechanical alloy. Metall Trans A 11A:1771–1775
Martínez-Ona R, Pérez MC (2000) Research on creep damage detection in reformer tubes by ultrasonic testing. In: Proceedings of 15th World congress on nondestructive testing. AIPnD, Roma
McVetty PG (1934) Working stresses for high temperature service. Mech Eng 56:149
Murakami S, Kawai M, Yamada Y (1990) Creep after cyclic-plasticity under multiaxial conditions for type 316 stainless steel at elevated temperature. J Eng Mater Tech 112:346–352
Narayan R, Green RE Jr (1975) Ultrasonic attenuation monitoring of fatigue damage in nuclear pressure vessel steel at high temperature. Materials evaluation, pp 25–36
Norton FH (1929) Creep of steel at high temperatures. McGraw-Hill, New York
Odqvist FKG (1966) Mathematical theory of creep and creep rupture. Clarendon Press, Oxford
Ogi H, Minami Y, Aoki S, Hirao M (2000) Contactless monitoring of surface-wave attenuation and nonlinearity for evaluating remaining life of fatigued steels. In: Proceedings of 15th World congress on nondestructive testing. AIPnD, Roma
Ohashi Y, Kawai M, Momose T (1986) Effects of prior plasticity on subsequent creep of type 316 stainless steel at elevated temperature. J Eng Mater Tech 108:68–74
Pandey MC, Mukherjee AK, Taplin DMR (1984) Prior deformation effects on creep and fracture in Inconel alloy X-750. Metall Trans A 15A:1437–1441
Piechnik S, Chrzanowski M (1970) Time of total creep rupture of a beam under combined tension bending. Inst J Solids Struct 6:453–477
Rabotnov YN (1969) Creep problems in structural members. North Holland Publishing Company, Amsterdam
Rees DWA (1981) Effects of plastic prestrain on the creep of aluminium under biaxial stress. In: Wilshire B, Owen DR (eds) Creep and fracture of engineering materials and structures. Pineridge Press, Swansea, pp 559–572
Sablik MJ, Augustyniak B (1999) Encyclopedia of electrical and electronics engineering. Magnetics methods on nondestructive evaluation. Wiley, Chichester
Sdobyrev VP (1959) Creep criterion for some high-temperature alloys in complex stress state. Izv AN SSSR Mekh and Mashinostr 6:12–19 (in Russian)
Szelążek J (2001) Advances in ultrasonic investigations of stresses. Report 4, IFTR, Warszawa
Trąmpczyński W, Kowalewski Z, (1986) A tension-torsion testing technique. In: Dyson B, Loveday M (eds) Techniques for multiaxial creep testing. Elsevier Applied Science, London and New York, pp 79–92
Trąmpczyński WA (1982) The influence of cold work on the creep of copper under biaxial states of stress. Acta Metall 30:1035–1041
Wilson RN (1973) The influence of 3% prestrain on the creep strength of Al-2.5% Cu-1.2% Mg alloys at 150 °C. J Inst Metals 101:188–196
Xia Z, Ellyin F (1993) An experimental study on the effect of prior plastic straining on creep behavior of 304 stainless steel. J Eng Mater Tech 115:200–203